Journal of Alloys and Compounds 1005 (2024) 176175

Contents lists available at ScienceDirect

Journal of Alloys and Compounds

journal homepage: www.elsevier.com/locate/jalcom

An alternative chlorine-assisted optimization of CdS/Sb_2Se_3 solar cells: Towards understanding of chlorine incorporation mechanism

Sajeesh Vadakkedath Gopi [a,*], Nicolae Spalatu [a,*], Atanas Katerski [a], Jaroslav Kuliček [b], Bohuslav Razek [b], Egor Ukraintsev [b], Markéta Šlapal Bařinková [b], Guillaume Zoppi [c], Raitis Grzibovskis [d], Aivars Vembris [d], Liga Ignatane [d], Malle Krunks [a], Ilona Oja Acik [a]

[a] Department of Materials and Environmental Technology, Tallinn University of Technology, Ehitajate tee 5, Tallinn, Estonia
[b] Faculty of Electrical Engineering, Czech Technical University in Prague, Technická 2, Prague 166 27, Czech Republic
[c] Department of Mathematics, Physics, and Electrical Engineering, Northumbria University, Newcastle-upon-Tyne NE1 8ST, United Kingdom
[d] Institute of Solid-State Physics, University of Latvia, Riga, Latvia

ARTICLE INFO

Keywords:
Vapor transport deposition
CdS chlorine assisted optimization
Secondary ion mass spectroscopy
Sb2Se3 thin film solar cell

ABSTRACT

The current strategies in the development of Sb_2Se_3 thin film solar cells involve fabrication and optimization of superstrate and substrate device architectures, with the preferable choice for TiO_2 and CdS heterojunction layers. For CdS-based superstrate cells, several studies reported the necessity to apply $CdCl_2$ or other metal halide-based post-deposition treatment (PDT), highlighting improvement of CdS/Sb_2Se_3 device efficiency. However, the need, effect, and mechanism of such PDT are very often not described. Additionally, the fact that many groups have not succeeded in demonstrating its benefits suggests that this strategy is not straightforward, requiring a deeper understanding towards a more unified concept. The present study proposes an alternative approach to the challenging $CdCl_2$ PDT of CdS in CdS/Sb_2Se_3 device, involving controllable Cl incorporation in CdS films by systematically varying the concentration of NH_4Cl in the CBD precursor solution from 1 to 8 mM. Structural and electrical characterizations are correlated with advanced measurements of Scanning Kelvin Probe, surface photovoltage, and atomic force microscopy to understand the impact of Cl incorporation on the properties of CdS films and CdS/Sb_2Se_3 devices. The validity of Cl incorporation in the CdS lattice and interdiffusion processes at the $CdS\text{-}Sb_2Se_3$ interface is confirmed by secondary ion mass spectrometry analysis. It is demonstrated that incorporation of 1 mM of NH_4Cl, as a Cl source in CBD CdS, can boost the PCE of CdS/Sb_2Se_3 by ~20 %. With this approach, we offer new perspectives on the optimization methodology for Cl-based CdS/Sb_2Se_3 device processing and complementary understanding of the physiochemistry behind these processes.

1. Introduction

Antimony selenide (Sb_2Se_3) - based thin film photovoltaics have gained a lot of interest due to its huge potential for the development of eco-friendly solar cells. This material boasts a range of appealing characteristics, including its non-toxicity, abundance, and cost-effectiveness. Additionally, it exhibits a favourable band gap (1.1–1.3 eV)[1,2] and a high absorption coefficient ($>10^4$ cm^{-1} in the visible part of the spectrum)[3], positioning Sb_2Se_3 as a top contender among emerging thin film absorber materials. Given that Sb_2Se_3 is a binary compound with a single-phase structure, the potential for secondary phase formation, which was observed in quaternary compounds like copper indium gallium selenide (CIGS)[4] or copper zinc tin sulfide (CZTS)[5,6], can now be readily mitigated. This makes the material easy to deposit as thin films using different techniques such as radio frequency sputtering (RF)[7,8], thermal evaporation (TE)[9], close-spaced sublimation (CSS)[10,11], and vapour transport deposition (VTD)[12]. Among these deposition techniques, VTD provides clear advantages with increased controllability of the deposition conditions and a very high deposition rate at high temperatures resulting in a columnar structure, an essential feature for charge transport in devices [13] with power conversion efficiency (PCE) up to 7.6 % in superstrate configuration using VTD method [14].

Over the past decades, there has been a growing interest in Sb_2Se_3 solar cell research, leading to notable improvements in their efficiency. Fig. 1a illustrates the advancements in Sb_2Se_3 solar cell efficiencies over

* Corresponding authors.
E-mail addresses: sajeesh.vadakkedath@taltech.ee (S.V. Gopi), nicolae.spalatu@taltech.ee (N. Spalatu).

https://doi.org/10.1016/j.jallcom.2024.176175
Received 10 June 2024; Received in revised form 12 August 2024; Accepted 25 August 2024
Available online 26 August 2024

the years, utilizing different buffer layers such as CdS, $CdCl_2$-treated CdS, and TiO_2. The corresponding highest reported efficiencies are 10.1 %, 8.4 %, and 7.6 %, respectively. This data indicates that highly efficient Sb_2Se_3 solar cells have been achieved with both untreated and $CdCl_2$-treated CdS buffer layers. From 2009–2024, there have been approximately 59 publications focusing on the use of CdS alone and 26 publications utilizing $CdCl_2$-treated CdS buffer layers in Sb_2Se_3 solar cells (Fig. 1b). These publications specifically include those that have completed the solar cell fabrication and reported their efficiencies. It is important to note that numerous other publications concentrate solely on the material aspects of the research and are excluded from this database. This comprehensive analysis highlights the significant progress made in Sb_2Se_3 solar cell research and underscores the ongoing efforts to optimize buffer layers for enhanced device performance.

Among various explored heterojunction partner/buffer layers such as TiO_2 [15,16], ZTO [17], ZnO [18], and SnO_2 [19] many research groups set the choice for CdS in developing Sb_2Se_3 solar cells. This is often justified by its easy deposition through the well-established chemical bath deposition (CBD) method, suitable band gap of ~2.5 eV, n-type conductivity, and optimum band alignment with Sb_2Se_3[11]. Z. Duan et al. [20] and X. Wen et al. [14] reported PCE's as high as 10.1 % and 7.6 % using substrate and superstrate configurations employing CdS as the buffer layer. It is worth mentioning that these remarkable PCE results were achieved using CBD-deposited CdS films, without the employment of additional post-deposition treatments (PDTs). However, many studies reported the necessity of PDTs, especially the need for $CdCl_2$ treatment in air at temperatures $\geq$ 400 °C for 5–10 min [21]. Such a PDT is very often reported by many groups as a key step for achieving reasonable PCE for superstrate configuration CdS/Sb_2S_3 thin film devices. Nevertheless, the provided mechanisms behind this PTD step are often ambiguous and mainly justified as a taken standardized step – transferred from CdTe thin film technology [21,22]. Independent of the employed PDTs strategy for CdS, several studies raised the concerns about intermixing phenomenon, occurring at the CdS-Sb_2Se_3 interface and being identified as one major limitation for the PCE of the CdS/Sb_2Se_3 device configuration [10]. It has been shown that this intermixing, primarily driven by the diffusion of Cd to Sb_2Se_3 or Se to CdS, leads to the formation of CdSe at the interface [23]. The role of CdSe at the interface remains contentious, with contradictory reports suggesting its beneficial effect on carrier transport or detrimental impact – as the formation of a barrier at the main heterojunction interface [14,15]. In this context, the role of $CdCl_2$ PDT in the presence of air ambient conditions has been also justified as a necessary step to control the extent of the intermixing effect at the interface [24]. In particular, the beneficial effect of oxygen during the PDT (without $CdCl_2$) has been proven, even at moderate annealing temperatures of 200 °C, by improving the stability of CBD CdS and thus, preventing the formation of excessive intermixing at absorber-buffer interface [25]. The impact of various metal halide-based PDTs (such as $CdCl_2$ and $AlCl_3$) on the properties of CdS and CdS/Sb_2Se_3 thin film solar cells properties has been investigated, aiming the control and optimization of both, intermixing as well as passivation of interface defects [21,26,27].

However, there is no consensus yet in the community on the beneficial or detrimental effects of these metal halide-based PDTs and if this processing step should be employed as a PDT or as a controllable chlorine incorporation at the stage of CBD CdS deposition followed by annealing in various environmental conditions. Related to chlorine incorporation into the CdS lattice, it is well established that this impurity acts as a n-type shallow dopant and depending on its concentration, can significantly impact the electron concentration in the n-type CdS deposited by any physical or chemical methods [28]. The validity of chlorine as an n-type dopant in Sb_2Se_3 was also confirmed by the synthesis of intrinsic Sb_2Se_3 crystals from metallic precursors and subsequent deliberate n-type doping by the addition of $MgCl_2$ [29]. It has been also reported that during the intermixing between CdS and Sb_2Se_3, Cd diffusion can convert p-type Sb_2Se_3 into n-type by introducing a donor defect [30].

On one hand, all these results suggest that the extent of intermixing (alloy formation at the CdS-Sb_2Se_3 interface) and diffusivity of Cl or Cd depends on the employed deposition techniques and processing temperatures of both, CdS and Sb_2Se_3 films in the thin film solar stack. On the other hand, it is suggested that metal halide-based PDTs have an important role in the intermixing/alloy formation at the interface and hence, in the formation of the n-n isotype or n-p type heterojunction at CdS-Sb_2Se_3 interface. The latter phenomenon will significantly impact the recombination processes at this interface and consequently, affect the PV parameters and final PCE of the device. Based on the literature analysis, it can be also depicted that there is no unified answer yet on whether the metal halide-based PDTs (in air at $\geq$400 °C) and/or chlorine doping of CdS are needed and effective for the CdS-Sb_2Se_3 interface and PCE of the final device. Although such a statement might raise tumultuous debates, it is based on the following justifications: (i) According to Fig. 1b a significant number of studies do not report either successful or unsuccessful results of $CdCl_2$ PDT (or any other metal halide-based PDT) on the CdS properties and PCE of CdS/Sb_2S_3 devices; this finding is valid, independent of the employed superstrate or substrate CdS-based Sb_2Se_3 cell configuration. (ii) On the other hand, a several studies report findings on the suitability and beneficial effect of

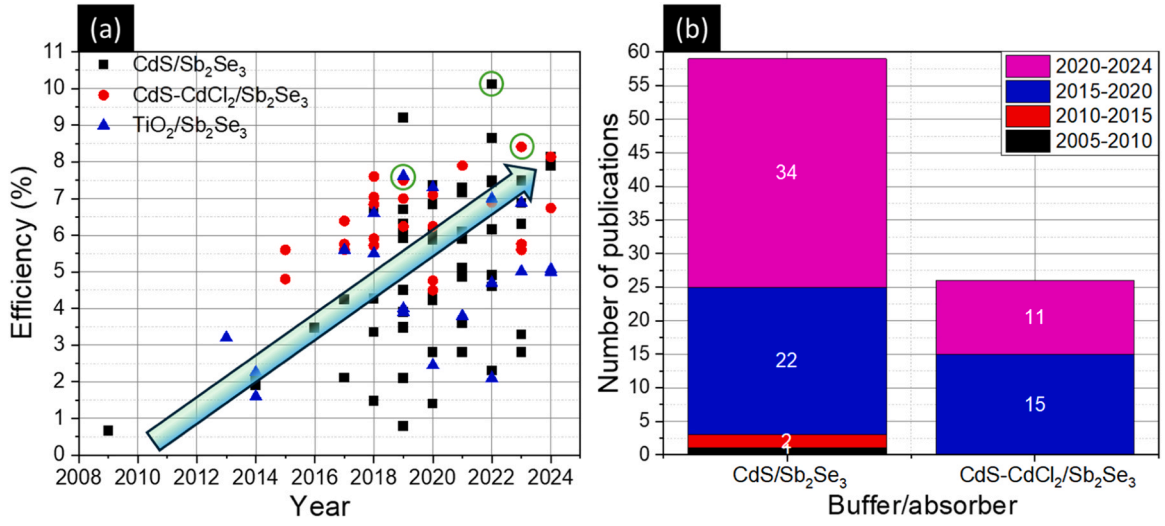

Fig. 1. Evolution of Sb_2Se_3 solar cell efficiency with CdS, $CdCl_2$-CdS and TiO_2 buffer layers and b) the corresponding number of publications.

$CdCl_2$-treated CdS on the PCE of Sb_2Se_3 solar cells.

At the same time, the developed knowledge on $CdCl_2$ PDT of CdS in CdTe demonstrated that this processing step promotes strong recrystallization (especially for CBD-deposited CdS) and improves the chemical stability of CdS towards the formation of suitable $CdS_{1-y}Te_y$ and $CdTe_{1-x}S_x$ alloy formation[31,32]. In one of our recent studies, we showed that standard $CdCl_2$ PDT of CBD CdS in the air at 400 °C is not a suitable approach for boosting the PCE of CdS/Sb_2Se_3 solar cells [10]. Therein close spaced sublimation was employed for the deposition of Sb_2Se_3 onto CBD CdS/FTO/glass and a very pronounced intermixing effect at the CdS-Sb_2Se_3 interface has been observed, limiting the final PCE of the device. Based on these cumulative results and considering the available knowledge on PDT $CdCl_2$ in CdTe, the transferability of the $CdCl_2$ processing step in air at 400°C to CdS (and consequently to the CdS-Sb_2Se_3 interface) is highly debatable and necessitates further systematic investigation and comprehensive understanding.

In this context, the present study proposes an alternative approach to the challenging $CdCl_2$ treatment of CdS in CdS/Sb_2Se_3 superstrate configuration cells. This approach involves incorporating Cl in a controllable manner into the CdS films by systematically varying the concentrations of NH_4Cl in the CBD precursor solution from 1 to 8 mM. Based on this precursor, a large series of CdS thin films were deposited onto both glass and glass/FTO substrates, and the impact of Cl incorporation on the properties of CdS films and CdS/Sb_2Se_3 was investigated. The incorporation of 1 mM of NH_4Cl, as a controllable chlorine source in CBD CdS, demonstrates a boost in the final PCE of CdS/Sb_2Se_3 by ~20 %. Routine structural and electrical characterization techniques are correlated with advanced measurements of Scanning Kelvin Probe, surface photovoltage, and atomic force microscopy to demonstrate and understand the impact of Cl incorporation on the properties of both CdS films and CdS/Sb_2Se_3 solar cells. We reveal that NH_4Cl introduced during the deposition does not change the CdS films structurally or morphologically but affects the film's electrical properties and energy levels resulting in a noticeable improvement in the solar cell performance. The validity of Cl incorporation into the CdS lattice and interdiffusion processes at the CdS-Sb_2Se_3 interface is confirmed by comprehensive secondary ion mass spectrometry depth profiles analysis of the CdS/Sb_2Se_3 heterostructure. Based on these systematic measurements, we provide a comprehensive discussion and analysis of the physicochemical processes responsible for the changes in the properties of CdS and CdS/Sb_2Se_3 solar cells, contributing with complementary knowledge on potential adjustments to methodologies for further development and optimization of emerging Sb_2Se_3-based thin film solar cells.

2. Experimental

2.1. Deposition of the CdS layer

CdS films were deposited on Flourine doped tin oxide (FTO) coated glass substrates (18 ×18 mm^2) by CBD. The substrates were cleaned using the standard procedure explained in the previously published article [25]. The deposition was carried out in a closed jar containing $CdSO_4$ (1 mM), $(NH_4)_2SO_4$ (0.7 M), NH_4Cl (0, 1, 2, 4 and 8 mM), NH_4OH (30 mM), and thiourea (10 mM) dissolved in de-ionized (DI) water at 79°C and stirred at 500 rpm. The chlorine content in the precursor was changed by the addition of different concentrations of NH_4Cl during the deposition. The deposition duration was optimized to be 10 min to get a 100 nm thick CdS layer. After deposition, the films were ultrasonicated in distilled water with a few drops of triethanolamine followed by washing again in distilled water and dried with a hot(100–150 °C) air gun. The prepared CdS samples were kept in a vacuum chamber and only taken outside for characterizations and deposition of Sb_2Se_3 by VTD.

2.2. Fabrication of CdS/Sb_2Se_3 solar cells

Sb_2Se_3 films were deposited on the glass/FTO/CdS substrates with different chlorine concentrations by VTD using a three-zone tubular furnace (Carbolite). Sb_2Se_3 granules of 5 N purity (Sigma Aldrich) were used as source materials. Initially, the quartz tube was evacuated using a combination of rotary and turbomolecular pumps (Pfeiffer vacuum) down to 10^{-5} mbar. The substrate-to-source distance was kept at 10 cm. The temperature of the source and substrate were ramped at 20 °C/min until it reached 500°C and 400°C, respectively. This temperature was kept for 5 min to obtain the desired thickness of 1 μm. After deposition, the furnace lid was opened, exposing the quartz tube to the ambient air. The vacuum pump was promptly shifted from turbo to rotary reducing the vacuum level to 10^{-2} mbar to stop the deposition of Sb_2Se_3 films. The superstrate configuration solar cells with glass/FTO/CdS/Sb_2Se_3/Au structure were completed by deposition of Au using thermal evaporation. Indium pads are used on top of the Au films during the device measurements.

2.3. Material and device characterizations

Structural properties of the CdS films and Sb_2Se_3 films were analyzed from X-ray diffraction (XRD) data measured by Rigaku Ultima IV using monochromator Cu Kα radiation (λ = 1.54 Å, 40 kV, 40 mA) equipped with D/teX silicon line detector in the 2Θ (Bragg-Bento) regime using 2Θ step of 0.04°, a counting time 2–10 s/step with sample rotation. The XRD patterns are then compared with JCPDS 01–074–9665 (CdS) and 015–0861 (Sb_2Se_3). The electrical properties (resistivity and carrier concentration) of CdS films were carried out at room temperature by Hall and Van der Paw controller H-50. The band gap of CdS films was calculated from UV vis spectroscopy (Jasco V-670 in 200–2500 nm) using a Tauc plot.

The contact potential difference (CPD) in the dark and under illumination of CdS and Sb_2Se_3 films was measured by a Scanning Kelvin Probe (SKP) system from KP Technology. The CPD data were recalculated to the work function values using the equation:

$$WF_{sample} = \left(CPD_{sample} - \quad CPD_{ref}\right) \times 10^{-3} + \quad WF_{ref} \tag{1}$$

As the WF reference (WF_{ref}), the Au reference sample from KP Technology was used. SKP measurements were done in a glove box using a grounded steel probe tip of 2 mm diameter. The CPD was measured in the dark-light-dark-light-dark cycle by switching solar simulator illumination (AM1.5 G filter, class AAA solar simulator HAL-C100, Asahi Spectra, Japan). CPD was measured as a function of time for 13.75 minutes (1250 data points). Multiple locations were tested on each sample. The surface photovoltage (SPV) was determined as the difference between WF_{light} and WF_{dark}. The second part of the SKP experiment was the mapping of WF across the scanned area of 4.89 × 4.89 mm^2 using a matrix of 12 × 12 points (hence 0.4075 mm per point). WF mapping was also performed in the dark and under the solar simulator illumination.

Topography of the CdS and CdS/Sb_2Se_3 films was measured by atomic force microscopy (AFM) using a NT-MDT Ntegra Prima instrument. Several Pt/Ir coated cantilevers with a resonance frequency of 75 KHz were used. The amplitude of the oscillation was 30 nm, with a setpoint of 65 %. The scan sizes were 1 × 1 and 2.5 × 2.5 μm^2 with scan speeds of 0.1 and 0.05 Hz respectively.

The surface morphology of the films was obtained using a scanning electron microscope (SEM) Zeiss EVO 10. The SEM images were acquired at 10 kV, magnification of 20 kX and working distance (WD) of 7.55 mm in the regime of secondary electrons (SE) using an off-beam detector.

The X-ray photoelectron spectroscopy (XPS) measurements were done using a Thermo Fisher ESCALAB Xi XPS/UPS system equipped with Al Kα radiation (hυ = 1486.6 eV) X-ray source.

Elemental depth profiling was acquired via secondary ion mass spectroscopy (SIMS). Positive and negative ion profiles were recorded using a hidden analytical IG20 gas ion gun and EQS1000 quadrupole detector. Samples were bombarded with Ar^+ ions (5 keV and 200 nA on the sample surface) and the beam was rastered over an area of 500 × 500 mm^2. A data gating of 10 % was applied for the analysis.

The superstate configuration solar cell performance was analyzed from the JV curve (AUTOLAB PGSTAT 30 and Oriel class A solar simulator 91159 A (100 mW/cm^2, AM1.5 G). The external quantum efficiency measurements were also carried out on the solar cells in the 300–1000 nm wavelength range using a light source (Newport 300 W Xenon lamp 69911), monochromator (Newport Cornerstone 260), and Si-calibrated detector (Merlin).

3. Results and discussions

As stated in the introduction part, in one of our recent studies, we showed that standard $CdCl_2$ PDT of CBD CdS in air at 400 °C is not a suitable approach for boosting the PCE of CdS/Sb_2Se_3 solar cells[10]. Therein, close-spaced sublimation (CSS) was employed for the deposition of Sb_2Se_3 onto glass/FTO/CBD - CdS and a very pronounced intermixing effect at the CdS-Sb_2Se_3 interface has been observed, limiting the final PCE of the device. At the same time, this might be the limitation of CSS technique in which a very close proximity between substrate and source (~10 mm) graphite blocks implies a very high supersaturated vapour phase near the samples. This effect combined with a high deposition rate (~0.5 μm/min) promotes conditions for a high chemical reactivity between CdS and Sb_2Se_3 and the formation of unfavourable alloy at the CdS-Sb_2Se_3 interface. This phenomenon appears to be less prominent when Sb_2Se_3 is deposited onto CdS using thermal vacuum evaporation and VTD techniques [33]. However, even for these techniques the effectiveness of $CdCl_2$ PDT of CdS buffer layer, in the air at 400 °C is still debatable. In this sense, we initially performed a series of experiments in which the $CdCl_2$ PDT in air at 400 °C was applied to CBD CdS followed by deposition of Sb_2Se_3 absorber by VTD. The impact of $CdCl_2$ PDT annealing duration on the solar cell performance is shown in fig S1 supplementary material. The results show that the longer the annealing time, the lower the solar cell performance. Independent of the annealing time the PCE is always lower compared to reference cell – without $CdCl_2$ treatment of CdS. We also investigated the impact of $CdCl_2$ PDT annealing temperature on the CdS/Sb_2Se_3 solar cells performance. The results are depicted in fig. S2 of supplementary material and it shows that regardless of the annealing temperature the PCE of the cells does not improve and the devices processed without $CdCl_2$ PDT of CdS still exhibit the highest PCE. Based on these results, we come with an alternative approach, proposing to incorporate chlorine in a controllable manner into the CdS films by systematically varying the concentrations of NH_4Cl in the CBD precursor solution from 1 to 8 mM. In this sense, we first analysed the impact of such processing approach on the properties of CdS films as described in Section 3.1 below.

3.1. Structural and morphological properties of CBD CdS films processed with different chlorine concentrations

To assess the influence of the incorporation of NH4Cl on the structural and morphological properties of CBD-deposited CdS films XRD, SEM, and AFM analysis were carried out on CdS films with 0, 1, 2, 4, and 8 mM NH4Cl concentrations. Fig. 1(a-e) shows the surface SEM images of the various CdS films. All films exhibited uniform and densely packed grains without any cracks and no significant changes in the CdS film morphology. There are reports on the modification of the morphology of CdS films due to doping of CdS with Cl- [28] as well as Ag ions [34] but here, since the concentration of the NH4Cl is rather small, a stable morphology was obtained for all the films.

The structural properties of the CdS films with different NH_4Cl concentrations were analyzed using XRD patterns, compared with standard pdf card 01–074–9665 [35] (Fig. 1f). The films exhibit hexagonal structure with distinct diffraction peaks at 25.2°, 26.8°, 28.5°, and 44.3° angles corresponding to the reflections from (100), (002), (101), and (110) planes, respectively. No discernible peaks associated with chlorine compounds, such as $CdCl_2$, were observed in the X-ray diffraction (XRD) pattern. This observation aligns with findings reported by Sivaraman et al. [36], who investigated the doping of chlorine into CdS and developed films via a spray coating method. Despite the lower chlorine concentration employed in our study compared to theirs, a similar trend was evident.

To investigate the effect of the NH_4Cl on the structural properties, the main (002) peak was separately analyzed (Fig. 2g). The films prepared with 0, 1, 2, and 4 mM NH_4Cl in the precursor had (002) peaks at nearly identical angles. In contrast, the CdS films with 8 mM NH_4Cl had a deviation to the lower 2Θ angle compared to that of 4 mM NH_4Cl CdS. In addition an interesting effect has been observed in which the (002) XRD peak is shifted towards higher 2Θ value as the NH_4Cl concentration increases from 0 to 4 mM. This effect has been observed previously in CdS films annealed in various ambient conditions [25] and can be explained by the presence of disorders in the lattice caused by incorporation of both Hydroxide group (OH) and chlorine into the CdS lattice during the deposition process. The displacement of (002) peak indicates that the chlorine was incorporated into the CdS lattice.

Fig. S3 (supplementary material) shows the AFM image of CdS deposited with 1 mM NH_4Cl in the precursor. Like the SEM images, the film has very uniform and well-packed grains.

3.2. Opto-electronic properties of CdS films processed with different chlorine concentrations

The bandgap of the CdS films deposited on the glass/FTO substrate with different NH_4Cl concentrations was calculated from Tauc plots based on UV-Vis measurements (Fig. 3a). The results reveal that there is a subtle decrease in the bandgap from 2.47 eV to 2.45 eV with the introduction of NH_4Cl and the concentration increases from 0 to 1 mM.

The band gap remains almost constant with the increase in the NH_4Cl concentration with slight changes of 0.1 eV. It is essential to emphasize that the observed changes in the bandgap were relatively small compared to the previous works involving high Cl^- doping levels.

The electrical properties (carrier concentration and resistivity) of the CdS films were obtained from hall measurements and the changes in these properties with an increase in NH_4Cl were investigated (Fig. 2b). All the films exhibit resistivity at the order of 10^4 Ω cm which was also reported by Hiie et al. [37]. Intriguingly, the resistivity of the CdS films had a pronounced surge from 3.6 $\times 10^4$ to 8.3 $\times 10^4$ Ω cm upon the introduction of 1 mM NH_4Cl in the bath. But then the resistivity sharply reduced to 3.3 $\times 10^4$ Ω cm when 2 mM NH_4Cl was used. After this, as the NH_4Cl concentration increases to 4 and 8 mM there is only a small step increase in the resistivity (3.3 $\times 10^4$ to 5.0 $\times 10^4$ Ω cm). The sharp decrease in the resistivity from 1 mM to 2 mM NH_4Cl might be due to the introduction of Cl^- ions into the CdS structure (not detected in XRD pattern (Fig. 2 f)), similarly, this can be also attributed to the sulfur deficiencies [38]. The incorporation of the added Cl atoms to the unoccupied sulfur vacancies increases the carriers which results in the decrease in resistivity.

Meanwhile, the carrier concentration of the CdS films has large variations corresponding to the change in NH_4Cl concentration. The maximum carrier concentration of 1.3 $\times 10^{14}$ /cm^3 was achieved for the films with 2 mM NH_4Cl. As the NH_4Cl concentration increases to 4 mM the carrier concentration remains almost similar but as the NH_4Cl concentration doubles to 8 mM the carrier concentration drops two orders of magnitude to 8.4 $\times 10^{12}$ /cm^3. The CdS films with 2 mM NH_4Cl have a maximum carrier concentration (1.318 × 10^{14} /cm^3) and the lowest resistivity (3.35 Ω cm) in the same way the CdS films 1 mM NH_4Cl have a maximum resistivity (8.37 Ω cm) and the lowest carrier concentration (3.4 $\times 10^{10}$ /cm^3). These significant changes in the electrical properties

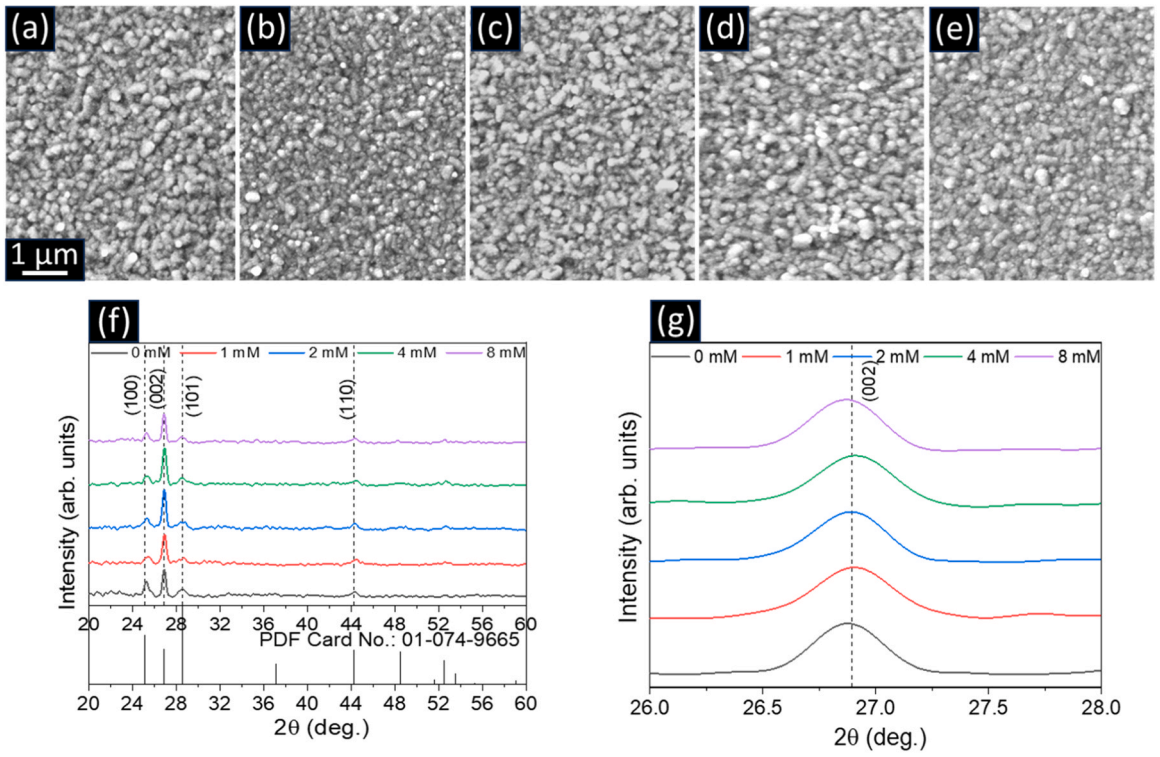

Fig. 2. (a-e) Surface SEM images of CdS films prepared with 0, 1, 2, 4, and 8 mM NH_4Cl in the CBD precursor, (f) XRD pattern of CdS with different NH_4Cl concentration, (g) Variation of (002) peak of CdS films with different NH_4Cl concentration.

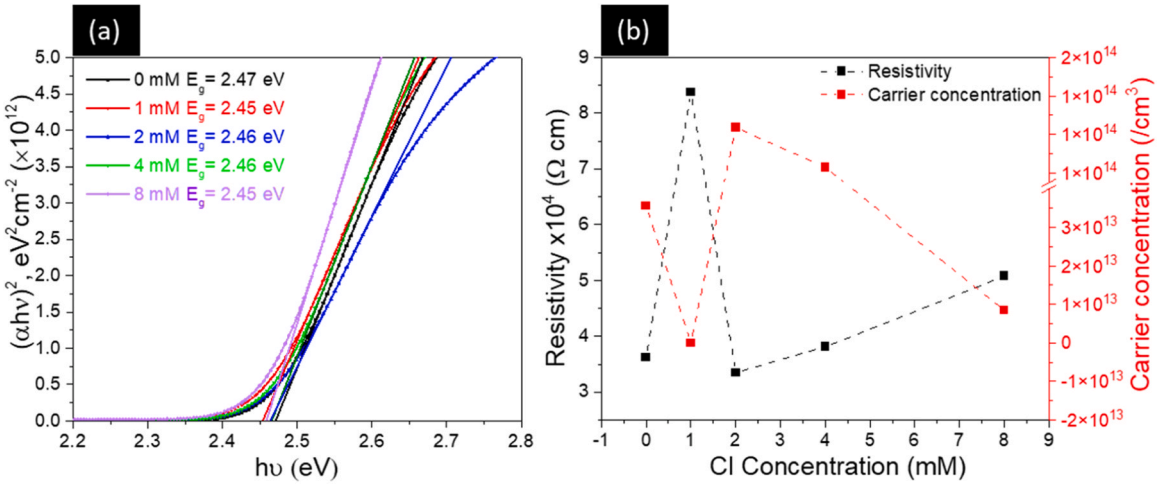

Fig. 3. (a) Tauc plots, showing the variation in bandgap of CdS films processed with 0–8 mM NH_4Cl concentration (b) electrical properties (carrier concentration and resistivity) of CdS films with different NH_4Cl concentration.

are good evidence of the incorporation of Cl into the CdS lattice. The more detailed explanation of the mechanism of chlorine incorporation on the electrical as well as on the device performance is explained in the later part of this paper.

As a step forward to better understand the energy levels of CdS films and the changes due to the introduction of NH_4Cl into it, the WF of the CdS films was measured in the dark-light-dark-light-dark cycle and the WF mapping was done in the dark and under the light across the 4.89 × 4.89 mm^2 area. Fig. 4(a, b, c, d, e) shows the WF maps of the CdS with 0, 1, 2, 4, and 8 mM NH_4Cl in the dark and Fig. 4(f, g, h, i, j) W.F. maps of same samples in order measured under the light. Fig. 4k shows the variation of WF and SPV with the change of NH_4Cl concentration, where WF is calculated as the average value from WF maps, and SPV is calculated from time-resolved measurements (Fig. S4 in the Supplementary material).

In Fig. 4a, WF for CdS with 0 mM NH_4Cl fluctuated between 4.42 and 4.55 eV in the dark, while WF decreased by ≈ 0.10 eV under illumination and fluctuated between 4.32 and 4.42 eV (Fig. 3f). A decrease in WF under light means positive photovoltage, thus generating holes on the surface. With the addition of 1 mM NH_4Cl, WF increased by 0.15 eV and fluctuated in the range of 4.50–4.60 eV (Fig. 4b). The WF values decreased under illumination and generated positive photovoltage (Fig. 3g). Furthermore, the surface charge is more homogenous compared to other samples. The sample CdS with 2 mM NH_4Cl WF range is 4.42–4.45 eV (Fig. 3c). Charge fluctuations can be partially influenced by sample morphology. Fig. 3d shows the WF map for CdS with 4 mM

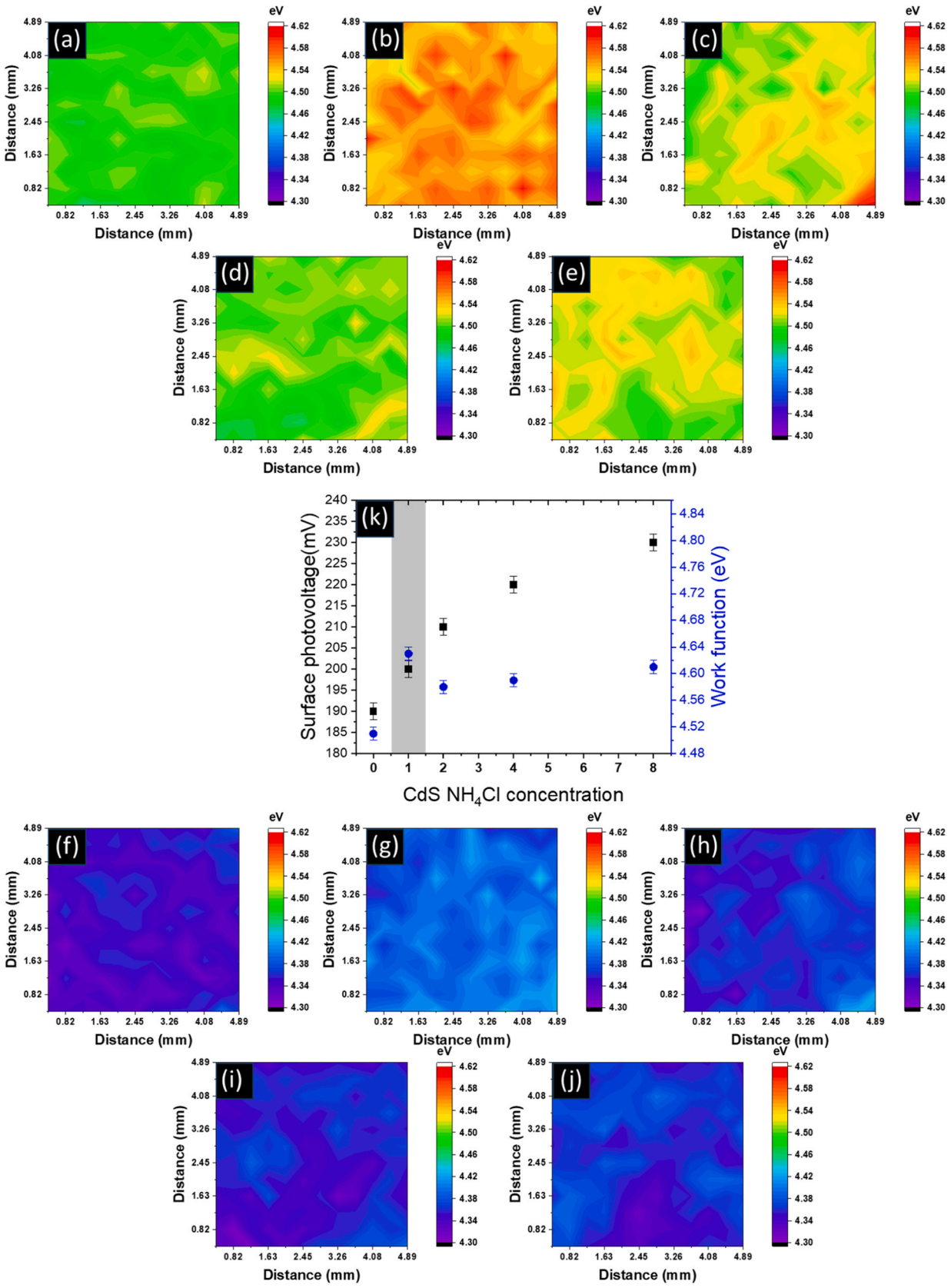

Fig. 4. (a, b, c, d, e) dark and (f, g, h, i, j) light condition work function distribution of CdS films at 0, 1, 2, 4, and 8 mM NH_4Cl in order (k) Variation of work function (WF) and surface photovoltage (SPV) with the change in NH_4Cl concentration.

NH_4Cl, where fluctuations of WF are in the similar range 4.42–4.45 eV as for CdS with 2 mM NH_4Cl. WF decreased under illumination for 0.15 eV, generating again positive SPV. The sample CdS with 8 mM NH_4Cl shows WF fluctuations between 4.46 and 4.56 eV (Fig. 3e). WF decreased under light by 0.20 eV to the range of 4.32–4.36 eV. In the overall trend we can see that the work function peaks at 4.63 eV when 1 mM NH_4Cl is introduced (increase by 0.12 eV). For higher NH_4Cl concentrations the values are similar, with small changes within 0.02 eV. The spatial distribution of work function across the sample surface is similar and uniform among the CdS films measured in the dark and under illumination, except for the CdS with 1 mM NH_4Cl which exhibits regions of higher work function compared to the other samples.

With the increase in the NH_4Cl concentration (1 mM to 2 mM) there was an abrupt increase in the carrier concentration (Fig. 2b). This is an indication of the incorporation of chlorine as a donor into the CdS lattice. From 2 mM to 8 mM NH_4Cl the carrier concentration decreases. It indicates that there is a compensation effect of chlorine by the creation of neutral complexes along with the side contribution of the OH impurities. Nevertheless, the surface photovoltage (Fig. 3k) of the CdS films increases steadily from 190 eV to 240 eV with an increase in the NH_4Cl concentration from 0 to 8 mM.

3.3. Elemental composition properties of CdS and CdS/Sb_2Se_3

The elemental characteristics of CdS films were investigated using X-ray Photoelectron Spectroscopy (XPS) and Energy Dispersive X-ray Spectroscopy (EDX) at varying NH_4Cl concentrations. The XPS spectra (depicted in Fig. S5a, b, and c) exhibited prominent Cd 3d peaks at 405.8 eV and 412.5 eV binding energies. Notably, there was no discernible detection of Cl 2p within the 190–210 eV range, suggesting that the chlorine incorporated during deposition is distributed deep within the film rather than residing on the surface. The peaks corresponding to Cd 3d and S 2p exhibited no significant variations with increasing NH_4Cl concentration. Similarly, Natalia et al. [39] also reported the non-varying XPS of CdS films with OH impurities.

Further confirmation was sought through EDX analysis performed on CdS films prepared with an NH_4Cl concentration of 8 mM (fig. S5 d). The peaks corresponding to O, S, Cd, and Sn were detected meanwhile Sn and O indicated the presence of oxygen and tin originating from the FTO substrate. Consequently, the elemental analysis corroborates the minimal chlorine content within the CdS film lattice. These results suggest that chlorine is either present in very low concentrations deep within the film or falls below the detection limit of the analytical instruments.

To investigate the elemental distribution and interdiffusion in the CdS/Sb_2Se_3 heterojunction solar cells, SIMS analysis was carried out on solar cells with 0, 1, and 8 mM NH_4Cl-CdS as buffer layers. Fig. 4a shows the distribution of Sb^{121}, Se^{80}, Cl^{35}, Cd^{114}, S^{32}, and F^{19} elements inside the solar cell structure with 1 mM-NH_4Cl. The distribution of constituents elements of the absorber (Sb_2Se_3) and buffer layer (CdS) was detected (Fig. 5a). The detection signals corresponding to Cl^{35} inside 1 mM NH_4Cl-CdS samples also confirm the incorporation of Cl inside the films, which was below the detection limit of EDX. To get insight into the possible intermixing of CdS and Sb_2Se_3 the Sb/Cd ratio (Fig. 5b) was calculated from the SIMS data for 0, 1, and 8 mM NH_4Cl-CdS samples.

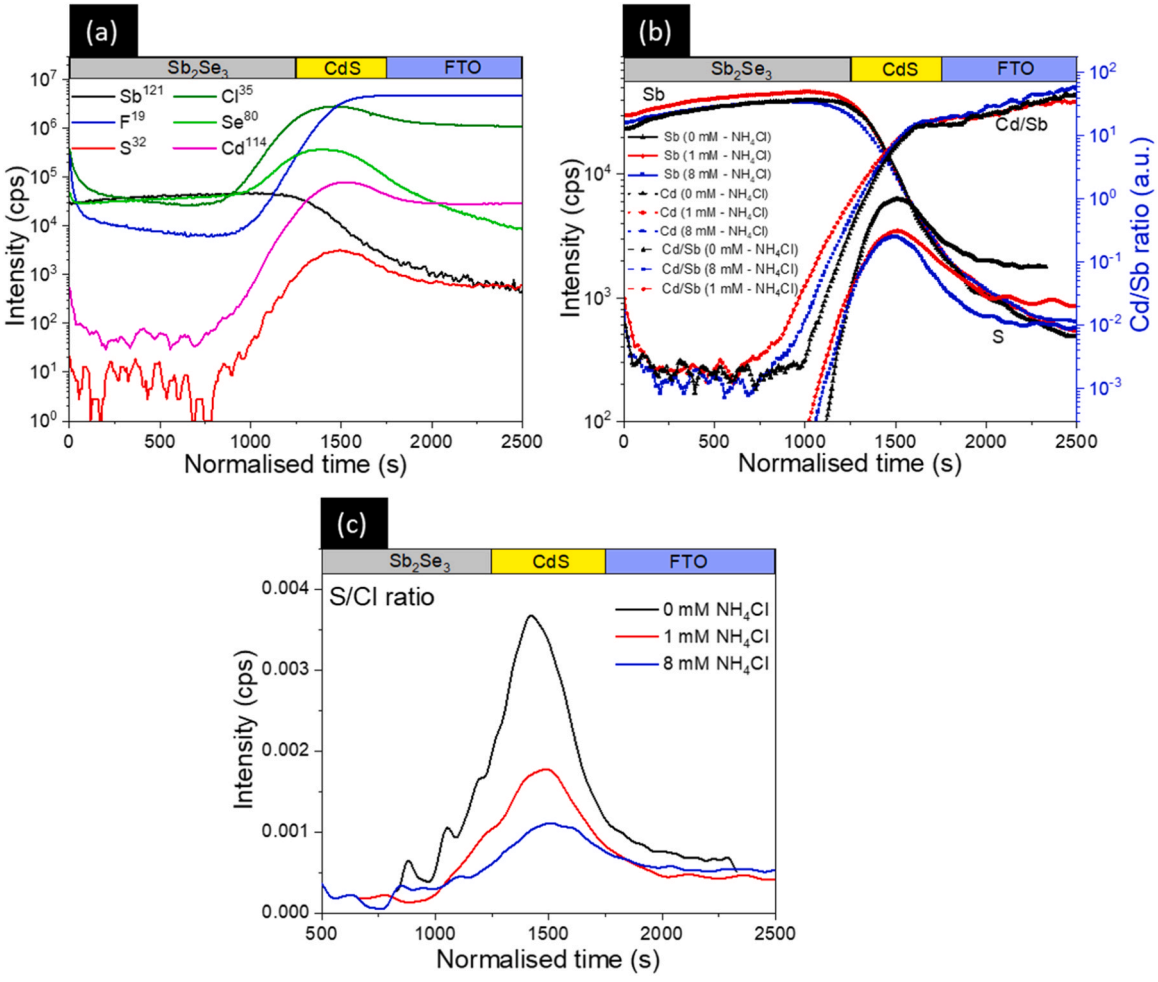

Fig. 5. Secondary ion mass Spectroscopy (SIMS) depth profiles, a) Sb, Se, Cd, S, Cl, and F elemental distribution in 1 mM NH_4Cl-CdS samples b) Cd/Sb ratio at NH_4Cl-CdS/Sb_2Se_3 interface c) S/Cl ratio of 0, 1, 8 mM NH_4Cl-CdS samples.

Both 1 mM and 8 mM samples showed a gentler slope at the CdS leading edge indicating Cd interdiffusion into the absorber when Cl is used. Interdiffusion appears not to be linearly correlated with the amount of Cl with the 1 mM NH_4Cl-CdS showing the largest intermixing. So clearly the CdS with 1 mM NH_4Cl has more interdiffusion of Cd to the absorber side which leads to more probability for intermixing and formation of CdSe at the interface. This might affect the solar cell performance, Wen X. et al.[14] reported that this intermixing leads to better lattice matching and lower defects, leading to an efficiency of 7.6 % using VTD as the deposition method for the Sb_2Se_3 deposition. Liang et al.[40] have also achieved an efficiency of 7.4 % through effective Sb_2Se_3 layer growth through VTD deposition followed by a post-selenisation procedure in substrate configuration CdS/Sb_2Se_3 solar cells. Meanwhile, other groups [10,15,41] have reported a detrimental effect on solar cell performance while depositing Sb_2Se_3 by CSS method. The impact of the Cl addition during the CBD process is shown in Fig. 5c where the S/Cl ratio is plotted. The S/Cl ratio is highest for 0 mM NH_4Cl-CdS and reduces with an increase in the NH_4Cl concentration, confirming the effective incorporation of Cl in the CdS films.

3.4. Structural and morphological properties of Sb_2Se_3 deposited on CdS films processed with various chlorine concentrations

As a step forward to solar cell preparation, the Sb_2Se_3 absorber films with a thickness of 1.023 μm were deposited by VTD on glass/FTO/CdS substrates, with varying NH_4Cl concentrations in the CdS films. The structural and morphological properties of the Sb_2Se_3 films were analyzed to study the effect of the change in CdS film on the absorber film. Fig. 6(a-e) shows the surface SEM images of Sb_2Se_3 films. It can be observed that the Sb_2Se_3 films are arranged very compactly without any porosity. However, the grains are not uniform, some with irregular size while others show a tower-like structure. This might be due to the substrate temperature irregularity obtained during VTD deposition. No significant changes in the morphology were observed for Sb_2Se_3 films due to changes in NH_4Cl concentration. The cross-section SEM image (Fig. 6 f) of 1 mM NH_4Cl-CdS/Sb_2Se_3 interface, confirms the columnar growth Sb_2Se_3 grains. The structural properties of the Sb_2Se_3 do not change with the difference in CdS films and all XRD spectra were identical to the example shown in Fig. 6 g for 1 mM NH_4Cl-CdS/Sb_2Se_3. The XRD pattern of Sb_2Se_3 deposited on CdS processed with various NH_4Cl concentration is presented in fig.S8 in the supporting material. The diffraction patterns were compared with standard data (JCPDS 15–0861) [13]. The diffraction peaks at 15.03°, 16.87°, 23.9°, 27.02°, 28.2°, 31.16°, 32.22°, 34.08°, 37.98°, 39.08°, 41.35°, 44.95°, 45.57° and 54.88° were detected corresponding to (020), (120), (130), (021), (211), (221), (301), (240), (041), (411), (250), (431), (002) and (061) planes. The XRD patterns have more intense (221) and (211) peaks indicating the tilted columnar grain growth of the Sb_2Se_3 films which was observed in the cross-section SEM image (Fig. 6 f) of the same sample.

Fig. S6 (supplementary material) presents the AFM image of the Sb_2Se_3 absorber film grown on CdS film with 1 mM NH_4Cl in the CBD bath. As with the SEM images, this gives a clear view of the overgrown grains in the film. The irregularities observed in the grain growth can be attributed to several factors, including non-uniform substrate temperature during rapid Sb_2Se_3 deposition. Additionally, the VTD deposition of the Sb_2Se_3 is happening at 400 °C. This could act as a post-deposition vacuum annealing process for the CdS films which leads to the out-diffusion of the residues and delay the growth of some grains.

3.5. Impact of the chlorine concentration in the CBD CdS precursor on the device performance

The Sb_2Se_3 solar cells with superstrate configuration (glass/FTO/CdS/Sb_2Se_3/Au) were fabricated and the changes in the device performance with a change in NH_4Cl concentration during the CdS deposition were analyzed. The solar cell parameters open circuit voltage (V_{OC}), short circuit current density (J_{SC}), fill factor (FF), and power conversion

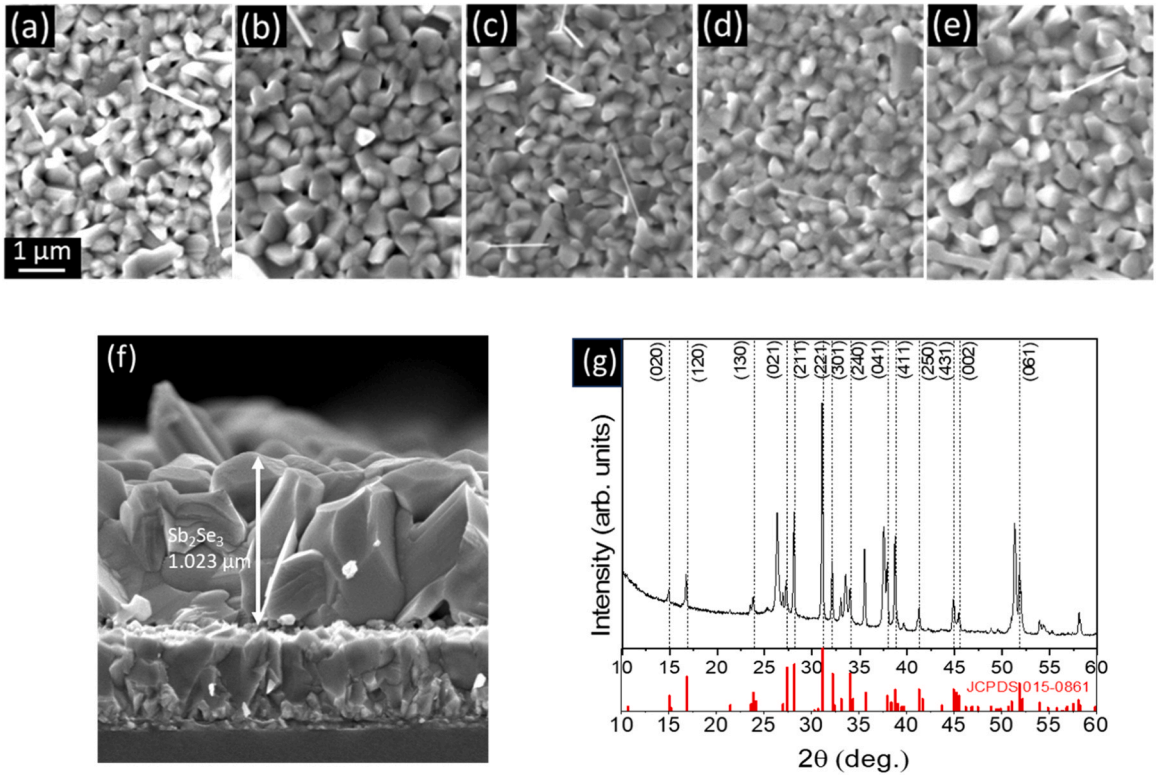

Fig. 6. (a-e) Surface SEM images of Sb_2Se_3 films prepared on CdS layers with 0, 1, 2, 4, and 8 mM NH_4Cl in the CBD precursor, (f) Cross-section SEM image of 1 mM NH_4Cl-CdS/Sb_2Se_3 structure (g) XRD pattern of Sb_2Se_3 on CdS with 1 mM NH_4Cl concentration.

efficiency (PCE) were extracted from the J-V characteristics (Fig. 7a-e).

The device parameters are influenced by the change in NH_4Cl concentration in the precursor during the CdS deposition. The V_{OC}, FF, and PCE of the solar cells were increased when 1 mM of NH_4Cl was introduced to the CdS films. The V_{OC} increases to 391.27 mV from 354.15 mV, FF increases to 52.4 % from 51.7 % and PCE increases to 4.6 % from 4.2 %. The highest PCE of 4.6 % was also obtained for the cells using a CdS layer buffer layer with 1 mM NH_4Cl. As the NH_4Cl concentration increases after 1 mM all the solar cell properties go down. The lowest PCE of 2.2 % was obtained for the solar cells with 8 mM NH_4Cl CdS buffer layers. The incorporated Cl has affected the solar cell parameters. The cells with maximum resistivity and minimum carrier concentration (1 mM NH_4Cl) CdS as buffer layer resulted in the best performance.

Similar to Fig. 4, WF maps and photovoltage were measured by SKP on the complete glass/FTO/CdS/Sb_2Se_3 devices. In this case on top Au contact and nearby bare Sb_2Se_3 surface. The results are summarized in fig. S7 and fig. S8 in the supplementary material. The most important observation is that the samples with 1 mM NH_4Cl show the largest photovoltage response and that the Au contact enhances this response, i.e., it significantly helps extract holes from the prepared solar cell.

The EQE response (Fig. 7 f) of solar cells shows steady efficiency in the 550 – 750 nm range. The integrated current density was also calculated from EQE and the values are in good agreement with those obtained from JV curves. The values of integrated J_{SC} are illustrated in fig. S9 in the supplementary material. The solar cells with CdS buffer layer deposited with 0 and 1 mM NH_4Cl have ~ 70 % response in the 550–750 nm region. As the concentration of the NH_4Cl in the CdS films increases the response steadily decreases, and the lowest efficiency of ~ 50 % was obtained for the cells using CdS films with 8 mM NH_4Cl. At the lower wavelength of the EQE spectra, a clear reduction in the response can be observed. This is one of the peculiar trends that has been reported by other researchers due to the intermixing effect between CdS and Sb_2Se_3 occurring as result of higher temperature deposition of Sb_2Se_3 absorber film. In our investigation, we observed a reduction in the EQE spectral response at lower wavelength (400–550 nm) for solar cells fabricated using 8 mM NH_4Cl-CdS/Sb_2Se_3 compared to those utilizing 1 mM NH_4Cl. The decrease in the EQE response at shorter wavelengths can be related with the greater stability of the CdS layer, and therefore to a greater parasitic absorption. This also agrees well with the SIMS results (Fig. 5a), where a higher degree of interdiffusion is revealed for the 1 mM NH_4Cl concentration. The mixing probably leads to a reduction of the CdS layer thickness and consequently of the parasitic absorption.

The better performance of the cell also depends on the best heterojunction between the buffer and the absorber films. CdS films are known for intermixing with the Sb_2Se_3 films, different research groups are trying to overcome these problems through different methods. There are reports on the incorporation of Al^{3+}[27,42], heterojunction annealing [43], and $CdCl_2$ thin-layer deposition[21,44,45] which resulted in better performance in the devices. The introduction of thin films such as TiO_2 also improved the efficiencies of the Sb_2Se_3 solar cell. In our case, it was the simple incorporation of Cl in the precursor/bath at 1 mM concentration that resulted in tremendously improved solar cell performance. This opens prospects for further fine-tuning and optimization of the CdS/Sb_2Se_3 heterojunction.

3.6. *Mechanism of chlorine incorporation in CdS and interrelation with CdS/Sb_2Se_3 device performance*

Based on the above observed systematic changes in the properties of CdS, Sb_2Se_3 films and solar cells, the following physicochemical processes are proposed:

(i) At the stage of CBD CdS processing: During the CBD deposition of CdS films, two concomitant processes occur in which both,

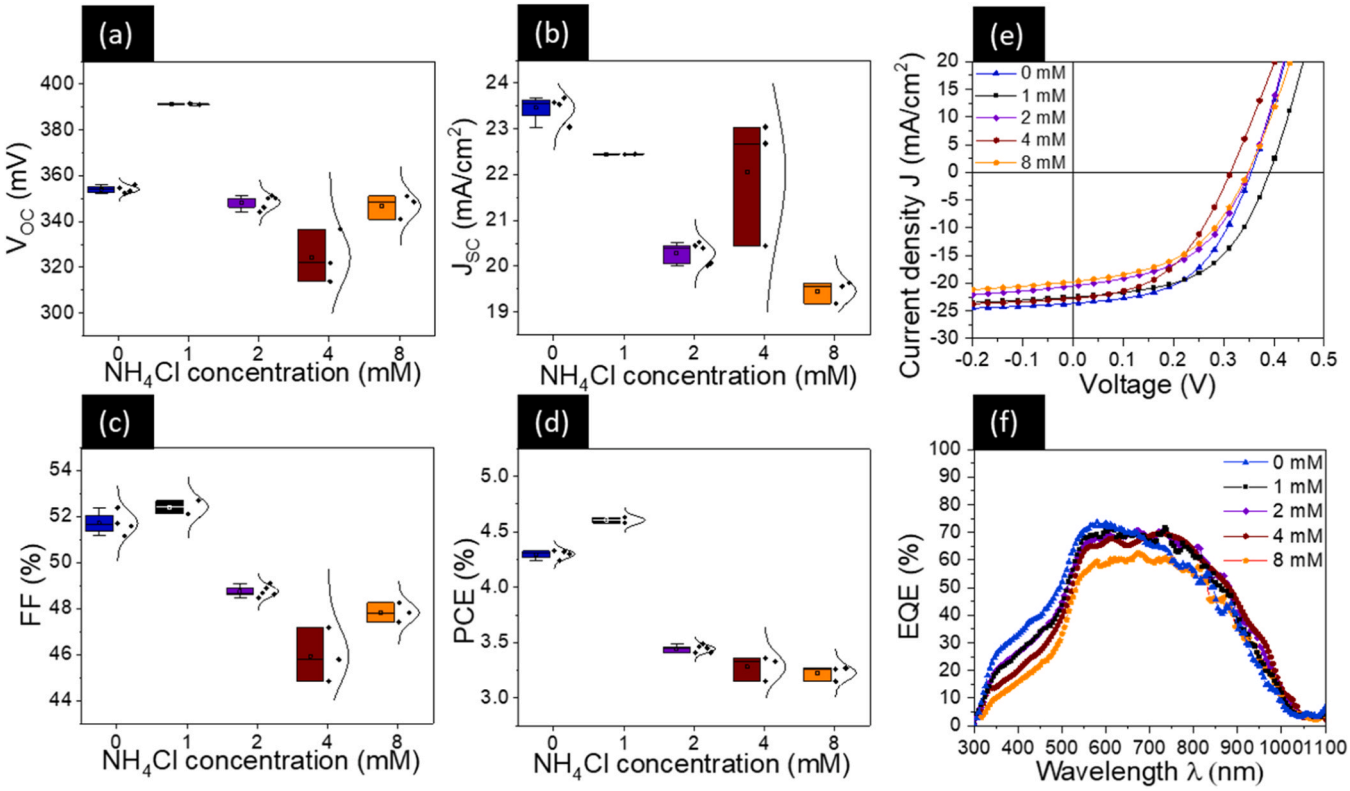

Fig. 7. (a) open circuit voltage (V_{OC}), (b) short circuit current (J_{SC}), (c) fill factor (FF), (d) power conversion efficiency (PCE), (e) JV characteristics and (f) external quantum efficiency (EQE) of CdS/Sb_2Se_3 solar cells with a change in NH_4Cl concentration in the precursor.

hydroxyl group and chlorine are incorporated into the CdS lattice according to the Eqs. 1–3:

$$nCdS + Cd(OH)_2 \rightarrow Cd_{n+1}S_n2(OH)_2V_{Cd} \quad (1)$$

$$2NH_4Cl + CdSO_4 \leftrightarrow CdCl_2 + (NH_4)_2SO_4 \quad (2)$$

$$nCdS + CdCl_2 \rightarrow Cd_{n+1}S_n2Cl_2V_{Cd} \quad (3)$$

According to Eq. 1, as a result of the chemical reaction, cadmium hydroxysulfide as a solid solution of cadmium hydroxide into CdS is formed and the OH group occupies the sulphur site into the CdS lattice, behaving as a shallow donor. On another hand, according to Eq. 2, the presence of NH_4Cl in the CBD precursor solution promotes formation of $CdCl_2$, leading to the incorporation of Cl into the CdS lattice and generating one V_{Cd} per every pair of incorporated Cl_S. Depending on the concentration of both hydroxyl group and chlorine in CdS, the generated V_{Cd}^{2-} can compensate the $(OH)_S^+$ and Cl_S^+, resulting in a low electron density of CdS.

Thus, at 0 mM NH_4Cl, the electron concentration in CdS film is entirely determined by the concentration of OH group which is incorporated into CdS on sulphur sites, generating an electron density of $\sim 3 \times 10^{13}$ cm^{-3} (Fig. 3b). An incorporation of 1 mM NH_4Cl in the CBD precursor seems to be a relatively low concentration to generate enough Cl_S^+ which would enhance the electron density. At such moderate Cl concentration and considering the incorporated $(OH)_S^+$, the concentration of double charged acceptor $(V_{Cd})^{2-}$ (which is generated by incorporation of both, and $Cd(OH)_2$ – Eq. 1, $CdCl_2$ – Eq. 3) appears to be high enough to compensate the shallow donors, resulting in enhanced resistivity and reduced electron density (Fig. 3b). An increase in the electron density of the films processed with 2 mM NH_4Cl in the CBD precursor can be explained by enhanced concentration of Cl_S^+ shallow donor defects which seems to be in higher concentration compared to $(V_{Cd})^{2-}$ at the given incorporated $CdCl_2$ amount. As the amount of NH_4Cl in the CBD precursor increases further, the electron density in CdS gradually drops (Fig. 3b) which can be related with the high Cl incorporation into the CdS lattice. Under these conditions, there is a high probability for Cl to occupy the interstitial states (acting as a p-type defect) into the CdS lattice, promoting high degree of compensation effect. Thus, these results indicate that depending on the amount of the NH_4Cl in the CBD precursor, the balance between $(OH)_S^+$ and Cl_S^+ is always shifted, governing, resistivity, electron density and work function in CdS films. However, this mechanism involves additional processes occurring during the stage of the Sb_2Se_3 absorber depositions by VTD, as follows.

At the stage of VTD Sb_2Se_3 absorber processing: During the Sb_2Se_3 absorber deposition at 400 °C (especially considering the time for ramping up the VTD source and substrate temperatures), CdS undergoes an annealing process, wherein the small CdS grains with high surface energy, undergoes intensive recrystallization by mass transport. On one hand, this recrystallization process induces decomposition and out diffusion of both chlorine and OH, resulting in their redistribution into the CdS lattice with a final impact on defect density and thus electrical properties of CdS buffer. On the other hand, according to SIMS analysis an interdiffusion of the elements at the main interfaces occurs, having a critical impact on the interface formation, including formation of interface defects and the quality of the n-p heterojunction. SIMS result confirms incorporation of Cl into the CdS and diffusion of Cd into Sb_2Se_3 absorber. The latest effect (of Cd diffusion into absorber) represent a major finding as many reports provided speculative hypothesis regarding Cd diffusion but without direct measurements proof. Some studies proposed the hypothesis that Cd act as donor defect in Sb_2Se_3 generating a rectifying junction in the spatial charge region [30]. Interestingly, in our case, for the device processed with 1 mM NH_4Cl CdS the diffusion of Cd was more pronounced (Fig. 5b). The same device showed the highest PCE suggesting that at 1 mM NH_4Cl the concentration of incorporated Cl into the CdS promotes a set of suitable condition for the formation of both, electrical properties of CdS as well as of the interdiffusion at the interface, resulting in the improved quality of the heterojunction and thus, device performance. It is worth mentioning that as an unexpected result, the SIMS analysis did not show any diffusion of chlorine into the absorber. So far, these results demonstrate that to achieve a beneficial impact of chlorine on the performance of CdS/Sb_2Se_3 device, the concentration of Cl should be relatively low, requiring careful incorporation control at both deposition stages, of CdS and Sb_2Se_3 absorber.

4. Conclusions

Exploring the influence of adding low concentration (1–8 mM NH_4Cl) of chlorine inside the CBD precursor on the characteristics of CdS films and CdS/Sb_2Se_3 solar cell device performance showed that the increase in chlorine concentrations does not affect the structural and morphological properties of CdS films whereas it significantly affects the electrical properties by changing carrier concentration and resistivity. There was an abrupt decrease in carrier concentration and an increase in resistivity with the introduction of 1 mM NH_4Cl. Additionally, bandgap of the CdS sample decreased with chlorine introduction from 2.47 eV to 2.45 eV. Photovoltage showed hole diffusion on CdS surface, on complete cells it showed pronounced positive effect of Au contact on effective charge collection. SIMS experiments detected increasing chlorine concentration and a higher interdiffusion of Cd into the absorber side was confirmed for devices with 1 mM NH_4Cl-CdS buffer layers. The morphology of Sb_2Se_3 films deposited via VTD on the CdS films with different NH_4Cl concentrations remained unchanged but an irregular grain height was observed in all films, this might be because of the irregular substrate temperature that occurred due to high vapor flow during the fast deposition. The Sb_2Se_3 films were (221) oriented regardless of CdS chlorine concentration. The devices with 1 mM NH_4Cl-CdS buffer layer had the best performance with 4.6 % PCE. A 20 % boost compared to the devices with 0 mM NH_4Cl-CdS. The performance of the devices decreases with an increase in chlorine concentration from 1 to 8 mM NH_4Cl. EQE measurements show a steady decrease in the spectral response in 500–800 nm region with an increase in NH_4Cl concentration. A detailed insight to the complex mechanism of the chlorine inside the CdS films and its effects on the device performance was provided opening new possibilities for the refinements in the methodologies of chlorine-assisted development and optimization of emerging CdS/Sb_2Se_3 solar cells.

Funding

All of the sources of funding for the work described in this publication are acknowledged below:

- Estonian Research Council project PRG627 “Antimony chalcogenide thin films for next-generation semi-transparent solar cells applicable in electricity producing windows”
- Estonian Research Council project PSG689 “Bismuth Chalcogenide Thin-Film Disruptive Green Solar Technology for Next Generation Photovoltaics”
- Estonian Ministry of Education and Research project (TK210; TK210U8) „Center of Excellence in Sustainable Green Hydrogen and Energy Technologies“,
- Engineering and Physical Sciences Research Council (UK) for funding through Reimagining Photovoltaics Manufacturing (EP/W010062/1)
- The European Union’s H2020 programme under the ERA Chair project 5GSOLAR grant agreement No 952509.
- COST Action Research and International Networking on Emerging Inorganic Chalcogenides for Photovoltaics (RENEW-PV), CA21148, supported by COST (European Cooperation in Science and Technology)

CRediT authorship contribution statement

Bohuslav Rezek: Writing – review & editing, Visualization, Validation, Supervision, Funding acquisition, Formal analysis, Data curation. **Markéta Šlapal Bařinková:** Formal analysis, Data curation. **Atanas Katerski:** Methodology, Formal analysis, Data curation. **Jaroslav Kuliček:** Writing – review & editing, Visualization, Validation, Formal analysis, Data curation. **Ilona Oja Acik:** Validation, Supervision, Project administration, Funding acquisition. **Nicolae Spalatu:** Writing – review & editing, Writing – original draft, Validation, Supervision, Methodology, Funding acquisition, Conceptualization. **Liga Ignatane:** Visualization, Formal analysis, Data curation. **Sajeesh Vadakkedath Gopi:** Writing – review & editing, Writing – original draft, Visualization, Validation, Investigation, Formal analysis, Data curation, Conceptualization. **Malle Krunks:** Writing – review & editing, Validation. **Raitis Grzibovskis:** Formal analysis, Data curation. **Aivars Vembris:** Formal analysis, Data curation. **Egor Ukraintsev:** Visualization, Formal analysis, Data curation. **Guillaume Zoppi:** Writing – review & editing, Visualization, Validation, Formal analysis, Data curation.

Declaration of Competing Interest

No conflict of interest exists.

Data availability

Data will be made available on request.

Acknowledgements

This study was funded by the Estonian Research Council projects PRG627 “Antimony chalcogenide thin films for next-generation semi-transparent solar cells applicable in electricity producing windows”, PSG689 “Bismuth Chalcogenide Thin-Film Disruptive Green Solar Technology for Next Generation Photovoltaics”, the Estonian Ministry of Education and Research project (TK210; TK210U8) „Center of Excellence in Sustainable Green Hydrogen and Energy Technologies“, and the European Union’s Horizon 2020 programme under the ERA Chair project 5GSOLAR grant agreement No 952509. The article is based upon work from COST Action Research and International Networking on Emerging Inorganic Chalcogenides for Photovoltaics (RENEW-PV), CA21148, supported by COST (European Cooperation in Science and Technology). The authors also acknowledge the Engineering and Physical Sciences Research Council (UK) for funding through Reimagining Photovoltaics Manufacturing (EP/W010062/1).

Intellectual property

We confirm that we have given due consideration to the protection of intellectual property associated with this work and that there are no impediments to publication, including the timing of publication, with respect to intellectual property. In so doing we confirm that we have followed the regulations of our institutions concerning intellectual property.

Appendix A. Supporting information

Supplementary data associated with this article can be found in the online version at doi:10.1016/j.jallcom.2024.176175.

References

[1] R. Tang, Z.H. Zheng, Z.H. Su, X.J. Li, Y.D. Wei, X.H. Zhang, Y.Q. Fu, J.T. Luo, P. Fan, G.X. Liang, Highly efficient and stable planar heterojunction solar cell based on sputtered and post-selenized Sb_2Se_3 thin film, Nano Energy 64 (2019), https://doi.org/10.1016/j.nanoen.2019.103929.

[2] Z. Li, X. Liang, G. Li, H. Liu, H. Zhang, J. Guo, J. Chen, K. Shen, X. San, W. Yu, R.E. I. Schropp, Y. Mai, 9.2%-efficient core-shell structured antimony selenide nanorod array solar cells, Nat. Commun. 10 (2019), https://doi.org/10.1038/s41467-018-07903-6.

[3] Y. Zhou, L. Wang, S. Chen, S. Qin, X. Liu, J. Chen, D.J. Xue, M. Luo, Y. Cao, Y. Cheng, E.H. Sargent, J. Tang, Thin-film Sb2Se3 photovoltaics with oriented one-dimensional ribbons and benign grain boundaries, Nat. Photonics 9 (2015) 409–415, https://doi.org/10.1038/nphoton.2015.78.

[4] Y.C. Lin, J.T. Huang, L.C. Wang, H.R. Hsu, Effect of Cu/(In+Ga) ratios on the secondary phases and the performance of Cu2InGa(S,Se)4thin film solar cells, J. Alloy. Compd. 690 (2017) 152–159, https://doi.org/10.1016/j.jallcom.2016.08.127.

[5] P. Prabeesh, I. Packia Selvam, S.N. Potty, Structural properties of czts thin films on glass and mo coated glass substrates: a rietveld refinement study, Appl. Phys. A Mater. Sci. Process. 124 (2018) 1–6, https://doi.org/10.1007/s00339-018-1649-7.

[6] P. Prabeesh, V.G. Sajeesh, I. Packia Selvam, M.S. Divya Bharati, G. Mohan Rao, S. N. Potty, CZTS solar cell with non-toxic buffer layer: a study on the sulphurization temperature and absorber layer thickness, Sol. Energy 207 (2020) 419–427, https://doi.org/10.1016/j.solener.2020.06.103.

[7] A. Dutta, R. Singh, S.K. Srivastava, T. Som, Tunable optoelectronic properties of radio frequency sputter-deposited Sb_2Se_3 thin films: role of growth angle and thickness, Sol. Energy 194 (2019) 716–723, https://doi.org/10.1016/j.solener.2019.11.016.

[8] A. Shongalova, M.R. Correia, J.P. Teixeira, J.P. Leitão, J.C. González, S. Ranjbar, S. Garud, B. Vermang, J.M.V. Cunha, P.M.P. Salomé, P.A. Fernandes, Growth of Sb_2Se_3 thin films by selenization of RF sputtered binary precursors, Sol. Energy Mater. Sol. Cells 187 (2018) 219–226, https://doi.org/10.1016/j.solmat.2018.08.003.

[9] X. Liu, J. Chen, M. Luo, M. Leng, Z. Xia, Y. Zhou, S. Qin, D.J. Xue, L. Lv, H. Huang, D. Niu, J. Tang, Thermal evaporation and characterization of Sb_2Se_3 thin film for substrate Sb_2Se_3/CdS solar cells, ACS Appl. Mater. Interfaces 6 (2014) 10687–10695, https://doi.org/10.1021/am502427s.

[10] N. Spalatu, R. Krautmann, A. Katerski, E. Karber, R. Josepson, J. Hiie, I.O. Acik, M. Krunks, Screening and optimization of processing temperature for Sb2Se3 thin film growth protocol: interrelation between grain structure, interface intermixing and solar cell performance, Sol. Energy Mater. Sol. Cells 225 (2021), https://doi.org/10.1016/j.solmat.2021.111045.

[11] H. Shiel, O.S. Hutter, L.J. Phillips, J.E.N. Swallow, L.A.H. Jones, T.J. Featherstone, M.J. Smiles, P.K. Thakur, T.L. Lee, V.R. Dhanak, J.D. Major, T.D. Veal, Natural Band Alignments and Band Offsets of Sb2Se3Solar Cells, ACS Appl. Energy Mater. 3 (2020) 11617–11626, https://doi.org/10.1021/acsaem.0c01477.

[12] R. Juškėnas, A. Naujokaitis, A. Drabavičius, V. Pakštas, D. Vainauskas, R. Kondrotas, Seed Layer Optimisation for Ultra-Thin Sb_2Se_3 Solar Cells on TiO2 by Vapour Transport Deposition, Materials 15 (2022), https://doi.org/10.3390/ma15238356.

[13] R. Krautmann, N. Spalatu, R. Gunder, D. Abou-Ras, T. Unold, S. Schorr, M. Krunks, I.O. Acik, Analysis of grain orientation and defects in Sb 2 Se 3 solar cells fabricated by close-spaced sublimation, Sol. Energy 225 (2021) 494–500, https://doi.org/10.1016/j.solener.2021.07.022.

[14] X. Wen, C. Chen, S. Lu, K. Li, R. Kondrotas, Y. Zhao, W. Chen, L. Gao, C. Wang, J. Zhang, G. Niu, J. Tang, Vapor transport deposition of antimony selenide thin film solar cells with 7.6% efficiency, (2021). https://doi.org/10.1038/s41467-018-04634-6.

[15] L.J. Phillips, C.N. Savory, O.S. Hutter, P.J. Yates, H. Shiel, S. Mariotti, L. Bowen, M. Birkett, K. Durose, D.O. Scanlon, J.D. Major, Current enhancement via a TiO 2 window layer for CSS Sb 2 Se 3 solar cells: performance limits and high V oc, IEEE J. Photo 9 (2019) 544–551, https://doi.org/10.1109/JPHOTOV.2018.2885836.

[16] M. Koltsov, R. Krautmann, A. Katerski, N. Maticiuc, M. Krunks, I. Oja Acik, N. Spalatu, A post-deposition annealing approach for organic residue control in TiO2 and its impact on Sb_2Se_3/TiO_2 device performance, Faraday Discuss. (2022), https://doi.org/10.1039/d2fd00064d.

[17] S. Chen, Y.A. Ye, M. Ishaq, D.Lou Ren, P. Luo, K.W. Wu, Y.J. Zeng, Z.H. Zheng, Z. H. Su, G.X. Liang, Simultaneous band alignment modulation and carrier dynamics optimization enable highest efficiency in Cd-Free Sb_2Se_3 solar cells, Adv. Funct. Mater. (2024), https://doi.org/10.1002/adfm.202403934.

[18] L. Wang, D.B. Li, K. Li, C. Chen, H.X. Deng, L. Gao, Y. Zhao, F. Jiang, L. Li, F. Huang, Y. He, H. Song, G. Niu, J. Tang, Stable 6%-efficient Sb_2Se_3 solar cells with a ZnO buffer layer, Nat. Energy 2 (2017), https://doi.org/10.1038/nenergy.2017.46.

[19] Z. Chen, H. Guo, C. Ma, X. Wang, X. Jia, N. Yuan, J. Ding, Efficiency improvement of Sb2Se3 solar cells based on La-doped SnO2 buffer layer, Sol. Energy 187 (2019) 404–410, https://doi.org/10.1016/j.solener.2019.05.026.

[20] Z. Duan, X. Liang, Y. Feng, H. Ma, B. Liang, Y. Wang, S. Luo, S. Wang, R.E. I. Schropp, Y. Mai, Z. Li, Sb_2Se_3 thin-film solar cells exceeding 10% power conversion efficiency enabled by injection vapor deposition technology, Adv. Mater. 34 (2022), https://doi.org/10.1002/adma.202202969.

[21] L. Wang, M. Luo, S. Qin, X. Liu, J. Chen, B. Yang, M. Leng, D.J. Xue, Y. Zhou, L. Gao, H. Song, J. Tang, Ambient CdCl2 treatment on CdS buffer layer for improved performance of Sb2Se3 thin film photovoltaics, Appl. Phys. Lett. 107 (2015), https://doi.org/10.1063/1.4932544.

[22] D.B. Li, X. Yin, C.R. Grice, L. Guan, Z. Song, C. Wang, C. Chen, K. Li, A.J. Cimaroli, R.A. Awni, D. Zhao, H. Song, W. Tang, Y. Yan, J. Tang, Stable and efficient CdS/Sb_2Se_3 solar cells prepared by scalable close space sublimation, Nano Energy 49 (2018) 346–353, https://doi.org/10.1016/j.nanoen.2018.04.044.

[23] T.P. Weiss, I. Minguez-Bacho, E. Zuccalà, M. Melchiorre, N. Valle, B. El Adib, T. Yokosawa, E. Spiecker, J. Bachmann, P.J. Dale, S. Siebentritt, Post-deposition

annealing and interfacial atomic layer deposition buffer layers of Sb_2Se_3/CdS stacks for reduced interface recombination and increased open-circuit voltages, Prog. Photovolt.: Res. Appl. (2022), https://doi.org/10.1002/pip.3625.
[24] J. Tao, X. Hu, J. Xue, Y. Wang, G. Weng, S. Chen, Z. Zhu, J. Chu, Investigation of electronic transport mechanisms in Sb_2Se_3 thin-film solar cells, Sol. Energy Mater. Sol. Cells 197 (2019) 1–6, https://doi.org/10.1016/j.solmat.2019.04.003.
[25] S. Vadakkedath Gopi, N. Spalatu, M. Basnayaka, R. Krautmann, A. Katerski, R. Josepson, R. Grzibovskis, A. Vembris, M. Krunks, I. Oja Acik, Post deposition annealing effect on properties of CdS films and its impact on CdS/Sb_2Se_3 solar cells performance, Front Energy Res 11 (2023), https://doi.org/10.3389/fenrg.2023.1162576.
[26] J. Zhou, X. Zhang, H. Chen, Z. Tang, D. Meng, K. Chi, Y. Cai, G. Song, Y. Cao, Z. Hu, Dual-function of $CdCl_2$ treated SnO_2 in Sb_2Se_3 solar cells, Appl. Surf. Sci. 534 (2020), https://doi.org/10.1016/j.apsusc.2020.147632.
[27] Y. Luo, G. Chen, S. Chen, N. Ahmad, M. Azam, Z. Zheng, Z. Su, M. Cathelinaud, H. Ma, Z. Chen, P. Fan, X. Zhang, G. Liang, Carrier transport enhancement mechanism in highly efficient antimony selenide thin-film solar cell, Adv. Funct. Mater. (2023), https://doi.org/10.1002/adfm.202213941.
[28] N. Maticiuc, J. Hiie, T. Raadik, A. Graf, A. Gavrilov, The role of Cl in the chemical bath on the properties of CdS thin films, Thin Solid Films (2013) 184–187, https://doi.org/10.1016/j.tsf.2012.11.107.
[29] T.D.C. Hobson, L.J. Phillips, O.S. Hutter, H. Shiel, J.E.N. Swallow, C.N. Savory, P. K. Nayak, S. Mariotti, B. Das, L. Bowen, L.A.H. Jones, T.J. Featherstone, M. J. Smiles, M.A. Farnworth, G. Zoppi, P.K. Thakur, T.L. Lee, H.J. Snaith, C. Leighton, D.O. Scanlon, V.R. Dhanak, K. Durose, T.D. Veal, J.D. Major, Isotype Heterojunction Solar Cells Using n-Type Sb_2Se_3 Thin Films, Chem. Mater. 32 (2020) 2621–2630, https://doi.org/10.1021/acs.chemmater.0c00223.
[30] Y. Zhou, Y. Li, J. Luo, D. Li, X. Liu, C. Chen, H. Song, J. Ma, D.J. Xue, B. Yang, J. Tang, Buried homojunction in CdS/Sb_2Se_3 thin film photovoltaics generated by interfacial diffusion, Appl. Phys. Lett. 111 (2017), https://doi.org/10.1063/1.4991539.
[31] I.O. Oladeji, L. Chow, C.S. Ferekides, V. Viswanathan, Z. Zhao, Metal/CdTe/CdS/Cd1−xZnxS/TCO/glass: a new CdTe thin film solar cell structure, Sol. Energy Mater. Sol. Cells 61 (2000) 203–211, https://doi.org/10.1016/S0927-0248(99)00114-2.
[32] A. Graf, N. Maticiuc, N. Spalatu, V. Mikli, A. Mere, A. Gavrilov, J. Hiie, Electrical characterization of annealed chemical-bath-deposited CdS films and their application in superstrate configuration CdTe/CdS solar cells. Thin Solid Films, Elsevier B.V., 2015, pp. 351–355, https://doi.org/10.1016/j.tsf.2014.11.003.
[33] H. Guo, Z. Chen, X. Wang, Q. Cang, X. Jia, C. Ma, N. Yuan, J. Ding, Enhancement in the efficiency of Sb2Se3 thin-film solar cells by increasing carrier concertation and inducing columnar growth of the grains, Sol. RRL 3 (2019), https://doi.org/10.1002/solr.201800224.
[34] S.R. Ferrá-González, D. Berman-Mendoza, R. García-Gutiérrez, S.J. Castillo, R. Ramírez-Bon, B.E. Gnade, M.A. Quevedo-López, Optical and structural properties of CdS thin films grown by chemical bath deposition doped with Ag by ion exchange, Opt. (Stuttg.) 125 (2014) 1533–1536, https://doi.org/10.1016/j.ijleo.2013.08.035.
[35] N. Maticiuc, J. Hiie, V. Mikli, T. Potlog, V. Valdna, Structural and optical properties of cadmium sulfide thin films modified by hydrogen annealing, Mater. Sci. Semicond. Process 26 (2014) 169–174, https://doi.org/10.1016/j.mssp.2014.04.031.
[36] T. Sivaraman, V. Narasimman, V.S. Nagarethinam, A.R. Balu, Effect of chlorine doping on the structural, morphological, optical and electrical properties of spray deposited CdS thin films, Prog. Nat. Sci.: Mater. Int. 25 (2015) 392–398, https://doi.org/10.1016/j.pnsc.2015.09.010.
[37] J. Hiie, T. Dedova, V. Valdna, K. Muska, Comparative study of nano-structured CdS thin films prepared by CBD and spray pyrolysis: annealing effect, Thin Solid Films 511–512 (2006) 443–447, https://doi.org/10.1016/j.tsf.2005.11.070.
[38] O. De Melo, L. Hernández, O. Zelaya-Angel, R. Lozada-Morales, M. Becerril, E. Vasco, Low resistivity cubic phase CdS films by chemical bath deposition technique, Appl. Phys. Lett. 65 (1994) 1278–1280, https://doi.org/10.1063/1.112094.
[39] N. Maticiuc, A. Katerski, M. Danilson, M. Krunks, J. Hiie, XPS study of OH impurity in solution processed CdS thin films, Sol. Energy Mater. Sol. Cells 160 (2017) 211–216, https://doi.org/10.1016/j.solmat.2016.10.040.
[40] G. Liang, M. Chen, M. Ishaq, X. Li, R. Tang, Z. Zheng, Z. Su, P. Fan, X. Zhang, S. Chen, Crystal growth promotion and defects healing enable minimum open-circuit voltage deficit in antimony selenide solar cells, Adv. Sci. 9 (2022), https://doi.org/10.1002/advs.202105142.
[41] X. Liu, C. Chen, L. Wang, J. Zhong, M. Luo, J. Chen, D.J. Xue, D. Li, Y. Zhou, J. Tang, Improving the performance of Sb_2Se_3 thin film solar cells over 4% by controlled addition of oxygen during film deposition, Prog. Photovolt.: Res. Appl. 23 (2015) 1828–1836, https://doi.org/10.1002/pip.2627.
[42] G. Chen, Y. Luo, M. Abbas, M. Ishaq, Z. Zheng, S. Chen, Z. Su, X. Zhang, P. Fan, G. Liang, Suppressing buried interface nonradiative recombination losses toward high-efficiency antimony triselenide solar cells, Adv. Mater. 36 (2024), https://doi.org/10.1002/adma.202308522.
[43] R. Tang, S. Chen, Z.H. Zheng, Z.H. Su, J.T. Luo, P. Fan, X.H. Zhang, J. Tang, G. X. Liang, Heterojunction annealing enabling record open-circuit voltage in antimony triselenide solar cells, Adv. Mater. 34 (2022), https://doi.org/10.1002/adma.202109078.
[44] M. Azam, Y.Di Luo, R. Tang, S. Chen, Z.H. Zheng, Z.H. Su, A. Hassan, P. Fan, H. L. Ma, T. Chen, G.X. Liang, X.H. Zhang, Organic chloride salt interfacial modified crystallization for efficient antimony selenosulfide solar cells, ACS Appl. Mater. Interfaces 14 (2022) 4276–4284, https://doi.org/10.1021/acsami.1c20779.
[45] H. Cai, R. Cao, J. Gao, C. Qian, B. Che, R. Tang, C. Zhu, T. Chen, Interfacial Engineering towards Enhanced Photovoltaic Performance of Sb2Se3 Solar Cell, Adv. Funct. Mater. (2022), https://doi.org/10.1002/adfm.202208243.

The Institute of Solid State Physics of the University of Latvia, has received funding from the European Union framework program Horizon 2020 H2020-WIDESPREAD-01-2026-2017-TeamingPhase2 within the framework of grant agreement No. 739508 of the CAMART2 project.